EUROPEAN ORGANIZATION FOR NUCLEAR RESEARCH

CERN-EP/99-149
10 September 1999

RICH detectors

E. Nappi
CERN, Switzerland and INFN, Sez. Bari, Bari, Italy

Abstract

Basic principles of the Ring Imaging CHerenkov (RICH) technique are given, the issues of designing devices based on such a technique and the factors which limit the particle discriminating power are discussed. The challenging designs adopted by current experiments are also reviewed.

Lectures given at the 8^{th} ICFA School on Instrumentation in Particle Physics (Istanbul, 1999)

1 Introduction

The first time I was involved in the development of a RICH detector was many years ago, namely in 1985. In that period, I was participating in the NA35 experiment at CERN and after two years of data-taking, the Collaboration wished to upgrade the apparatus with a device having particle identification (PID) capability. When a RICH detector was proposed, frankly I must say that my first opinion on this technology was negative: a nasty photosensitive vapour called TMAE was addressed in its design and the pattern recognition seemed quite complicated with strange patterns to reconstruct. Moreover, the use of TMAE required a quite complicated detector geometry with blind electrodes and operation at high temperature. Despite my first judgment, by studying better the anticipated performance, it became clear to me that this technique was extremely powerful. The separation power reachable is unmatched among the current alternative technologies, therefore I decided to commit myself to the construction of a detector of that kind and after that many others followed. And now here I am, trying to fascinate you by showing how RICH detectors are impressively efficient in particle identification.

The RICH detector, conceived by A. Roberts [1], is the last born in the large family of devices based on the detection of Cherenkov radiation, named after the Russian physicist who discovered that charged particles moving through a medium with a velocity greater than the local phase velocity of light emanate a glow analogous to a sonic shock wave.

The spectrum and intensity of Cherenkov radiation can be calculated with high accuracy in terms of the classical theory of electromagnetism. The theoretical interpretation assumes that the atoms of the medium become polarized in the region along the charged particle track. Owing to the transient nature of this phenomenon, polarized atoms relax back to equilibrium by emitting a short electromagnetic pulse. When the velocity of the particle does not exceed the local phase velocity of light, the emitted electromagnetic pulses interfere destructively because of the symmetrical distribution of the polarization field. Otherwise, a coherent wavefront, at a specific angle θ_c with respect to the particle direction, is produced when the particle moves faster than light since only in this case the polarization field is asymmetric along the particle track. The resulting radiation covers a band of frequencies corresponding to the different Fourier components of the electromagnetic pulses emitted by the medium dipoles. Although Cherenkov radiation is feeble, few hundred photons against the many thousands of photons emitted in scintillating material, the use of its directional properties is a powerful tool for the identification of charged particles.

This paper is based on two lectures given at the 8^{th} ICFA School on Instrumentation in Particle Physics (Istanbul, 1999) and consists of three parts. In the first part, the field is introduced by starting with an historical overview and later with the basic principles of the Cherenkov effect. The second part, after having outlined the different detector schemes, deals with the analysis of RICH performance with a detailed discussion on measurement errors. The third part describes the components of a RICH detector, and their main applications in current and future experiments are given.

The present paper is not meant to cover all aspects of the RICH technique: electronics and pattern recognition are two important issues that have been deliberately left out because of the limited time allocated to the lectures. There are a number of comprehensive textbooks for further reading, the most significant being listed in Ref.[2]. Recently proposed new ingenious detector schemes, like the DIRC counter, are also not mentioned in the

present paper. Interested readers are referred to the Proceedings of the successful series of Workshops [3] devoted to Cherenkov light imaging since they represent an inexhaustible and updated source of information.

2 Historical overview

During the systematic work of reformulation of the Maxwell theory, anticipating by almost fifty years the experimental achievement of P. A. Cherenkov, Oliver Heaviside [4] showed that charged particles moving faster than light in vacuum emit an electromagnetic radiation whose wavefront propagates at a fixed angle with respect to the particle direction.
Although Heaviside made a wrong starting hypothesis since the condition of superluminality is not achievable in vacuum, his achievement is correct because the speed of charged particles moving in a dielectric medium with a refractive index larger than one can exceed the local phase velocity of light. Indeed, as early as 1919 M. Curie observed a faint blue light coming from concentrated solutions of radium in water. In 1934, the Russian P. A. Cherenkov, trying to understand the origin of the weak luminescience that salt solutions emit when struck by gamma rays, published a paper in which he proved that the light emission was caused by Compton electrons moving quickly through the liquid and showed the relationship between the emission angle and the refractive index of the medium [5].
In 1937, Frank and Tamm formulated the theory of the Cherenkov effect and predicted the radiation spectrum by applying the principles of classical electrodynamics [6]. The quantum formulation of such a theory was elaborated by Ginsburg [7] a few years later.
In 1958, Cherenkov, Frank and Tamm were jointly awarded the Physics Nobel prize for the discovery and interpretation of 'Cherenkov radiation'.

The capability of using the Cherenkov radiation for PID, was already clear to its discoverer in 1937 [8]. In the early days, distilled water was used as radiator and photographic emulsions or the researcher eyes as photodetector.
A major breakthrough in this technique was provided in the 1940s by the availability of photomultipliers capable of detecting feeble light with high efficiency and fast response.
Since 1951, when Jelley developed the first device specifically for a physics experiment [9] employing photomultipliers, several other detectors have been designed and built for both nuclear physics and particle physics experiments and for astrophysics applications as well. Cherenkov detectors played a fundamental role in important high energy physics achievements, for example in the discovery of the antiproton [10].

The idea to discriminate particles by differentiating between different values of the emission angle θ was conceived by A. Roberts in 1960 [1] and proved to be an extremely powerful method for identifying particles, as T. Ypsilantis and J. Seguinot [11] practically demonstrated in 1977 by imaging Cherenkov photons directly in a gaseous photodetector. This technique was named RICH: an acronym for "Ring Imaging CHerenkov" coined by T. Ekelof as a good omen for the funding situation of the experimental group involved in the realization of such a counter [12].
In 1982, a RICH device was for the first time installed in a high-energy physics experiment (E605 at Fermilab [13]), many others have been built since then. More recently, considerable advances in the technologies associated with photodetectors have extended the potentiality of such devices. As a result a renewed development of RICH counters is taking place.

3 Properties of Cherenkov radiation and basic formulae

The properties of Cherenkov radiation are contained in the following simple equation: [1)]

$$\cos\theta_c = \frac{1}{n\beta} \tag{1}$$

which provides the emission angle θ_c of Cherenkov photons in terms of the velocity of the charged particle β, in units of the speed of light, and the refractive index n of the medium. Since $|\cos\theta_c| \leq 1$, there exists a velocity threshold, expressed by the Lorentz factor

$$\gamma_t = (1 - 1/n^2)^{-\frac{1}{2}}. \tag{2}$$

When the velocity of the particle approaches the velocity of light in vacuum ($\beta \to 1$), θ_c takes the maximum value $\theta_{max} = \arccos 1/n$.
Eq.(1) alone, contains the two basic properties of the Cherenkov radiation that are exploited in practice, i.e. the existence of a threshold momentum and the peculiar direction of emission at an angle depending on the particle velocity.

For any practical purpose, the spectral dependence of the radiation must be taken into account. Frank and Tamm's equation describes the energy radiated per unit path length dx by a particle of charge Ze:

$$\frac{d^2W}{dxd\omega} = \frac{Z^2e^2\omega}{c^2}\left(1 - \frac{1}{\beta^2n^2(\omega)}\right), \tag{3}$$

where, due to the chromatic dispersion of the optical medium, n is a function of the radiation frequency ω. When integrated over the radiating path length L

$$\frac{dW}{d\omega} = \frac{LZ^2e^2\omega}{c^2}\left(1 - \frac{1}{\beta^2n^2(\omega)}\right). \tag{4}$$

We deduce that the energy loss because of Cherenkov effect is much lower than the ionization energy loss. Actually, if we consider an electron that moves with $\beta \simeq 1$ across a 1 cm of water ($n = 1.33$), in the spectral range $\lambda = 400 - 700\ nm$ the electron loses about 500 eV by the Cherenkov effect, whilst its energy loss by ionization is 2 MeV.

The number N of Cherenkov photons emitted with energy $\hbar\omega$ is a fundamental quantity for the detector design. It is easily deducible from Eq.(3):

$$N = \frac{LZ^2\alpha}{c}\int\left(1 - \frac{1}{\beta^2n^2(\omega)}\right)d\omega \tag{5}$$

or

$$N = 2\pi LZ^2\alpha\int_{\beta n>1}\left[1 - \left(\frac{\beta_t(\lambda)}{\beta}\right)^2\right]\frac{d\lambda}{\lambda^2}, \tag{6}$$

where α is the fine structure constant.
It follows that in 1 cm of material with a refractive index n, the number of photons emitted in the spectral range of 1 eV by a particle of charge Z moving with a $\beta \simeq 1$ is given by

$$N(cm^{-1}eV^{-1}) = 370Z^2\left(1 - \frac{1}{n^2}\right). \tag{7}$$

[1)] By taking into account the quantum theory of Cherenkov effect, the recoil of the charged particle of momentum p slightly modifies the classical Cherenkov equation by providing an additive term that is completely negligible for any practical application. The complete equation is:
$\cos\theta_c = \frac{1}{n\beta} + \frac{h}{\lambda p}\frac{n^2-1}{2n^2}$, where λ is the Cherenkov photon wavelength.

The total number of photons emitted depends upon the wavelength integration, but in general, as Eq.(7) indicates, the number of photons emitted per unit length and per unit energy is a constant, where there are no absorption bands close to the interesting frequency range. This constant is just the mean of the Poisson distribution in the number of photons, since it is an inherently statistical process.
In summary:
a) energy loss for Cherenkov radiation is of the order of keV/cm;
b) the amount of Cherenkov radiation is proportional to the square of the particle charge and it is independent on the particle mass;
c) the photon yield per unit of wavelength interval $d\lambda$ is proportional to $d\lambda/\lambda^2$, consequently most of the photons are emitted in the UV region;
d) equal number of photons per unit path per unit frequency interval.

4 Particle identification with Cherenkov detectors

A particle is univocally identified by its mass and electrical charge. The mass is provided by measuring at least two out of the three correlated quantities: momentum, kinetic energy and velocity. Practically, the choice is restricted to the momentum and velocity, in fact $p = mc\gamma\beta$.
The precision with which the mass is determined is given by

$$\left(\frac{dm}{m}\right)^2 = \left(\gamma^2\frac{d\beta}{\beta}\right)^2 + \left(\frac{dp}{p}\right)^2. \tag{8}$$

If the momentum p is relatively well measured, then the resolution of particles with masses m_1 and m_2 requires a velocity resolution, $\Delta\beta$, given by[2)]

$$\frac{\Delta\beta}{\beta} \simeq \frac{m_1^2 - m_2^2}{2p^2}. \tag{9}$$

Actually, the deflection of the particle trajectory in a suitable static magnetic field provides the charge sign and the momentum value, whilst the velocity is achieved by means of one of the following methods: energy loss, time of flight (TOF), detection of Cherenkov radiation and detection of transition radiation.
As Fig. 1 shows, in order to separate kaons from pions already in the momentum range of a few GeV/c the velocity resolution must be better than a few percent. Such a precision can be achieved only by Cherenkov counters. Indeed, it can be easily proved that the PID capability of a 1 m long TOF system with an excellent time resolution of 50 ps is limited to momenta below 1.5 GeV/c when a 3σ mass separation is required.

4.1 Threshold counters

By plotting the Cherenkov angle as a function of the particle velocity β, one realizes that the greatest sensitivity is provided by measuring the angle close to the threshold where $d\theta/d\beta$ is large (Fig. 2). However, the drawback is that the few photons emitted near the emission threshold cause the measurement of the Cherenkov angle to be affected by a large statistical error. Consequently the most effective way to exploit the threshold effect is achieved by counting the number $n_{p.e.}$ of detected photoelectrons. Near threshold

[2)] from $m_1^2 - m_2^2 = p^2\frac{\Delta\beta(\beta_1+\beta_2)}{(\beta_1\beta_2)^2}$

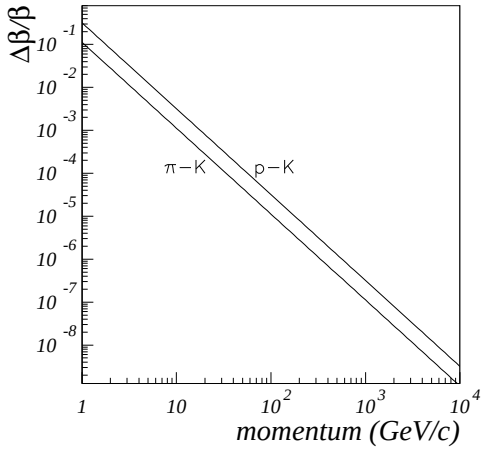

Figure 1: Resolution in velocity required to separate two particle species as a function of their momentum.

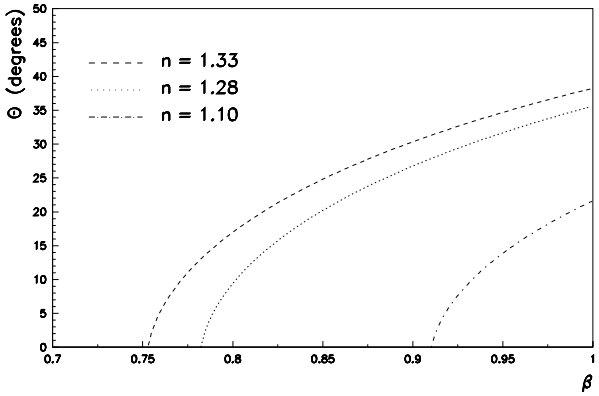

Figure 2: Variation of Cherenkov angle θ with particle velocity β for three different refractive indices: n=1.33 (water), n=1.28 (liquid perfluorohexane) and n=1.1 (aerogel). Emission angle changes rapidly close to the velocity threshold, its variation flattens as particle velocity increases.

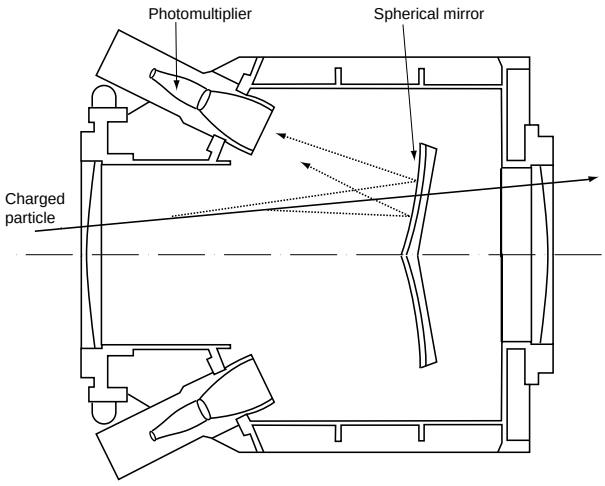

Figure 3: Schematic layout of a threshold Cherenkov detector.

$n_{p.e.} \simeq 0$, therefore the probability of not observing a signal is evaluated by means of Poisson distribution, $P(0) = e^{-n_{p.e.}}$, which gives an efficiency:

$$\epsilon = 1 - e^{-n_{p.e.}}. \tag{10}$$

This method is exploited in Cherenkov threshold detectors which employ a specific radiator medium whose refractive index n is chosen in such a way that radiation is only emitted when particles move through it with a speed exceeding c/n, thus allowing them to be separated from slower particles ('below threshold')(Fig. 3). Equation (10) implies that to keep the detector inefficiency at the level of 10^{-2} at least 4.5 photoelectrons must be detected on average.

A 'modern' version of the Threshold Cherenkov detector was proposed by F. Piuz [14] in 1995 for performing the hadron identification in the 3-8 GeV/c momentum range in the CERN-NA44 heavy ion experiment. The device, called TIC (Threshold Imaging Cherenkov), exploits the property of a gaseous wire chamber equipped with a UV sensitive pad-segmented cathode to localize with high spatial accuracy Cherenkov photons. Oppositely to the traditional threshold counters, TIC can be employed in experiments with several particles in the detector acceptance (Fig. 4).

4.2 DISC counters

A significant step in the application of Cherenkov radiation to PID took place at the beginning of 1970s, when Litt and Menieur [15] invented the Differential Isochronous Self Collimating detector, named DISC. By taking into account the formidable accuracy achieved in the past, as good as $\Delta\beta/\beta = 10^{-7}$, DISC is still, so far, the most precise device ever built for measuring the speed of particles in primary beams.

A DISC counter is an improved version of Differential Cherenkov counters where photons are focused onto a matrix of photomultipliers placed behind an annular diaphragm by means of a spherical mirror. Consequently, the photomultipliers provide ring imaging only for those particles that emit Cherenkov light in the diaphragm aperture angle. The better angle resolution achieved by DISC counters is obtained by implementing a specifically designed optics just immediately in front of the diaphragm, with the aim of

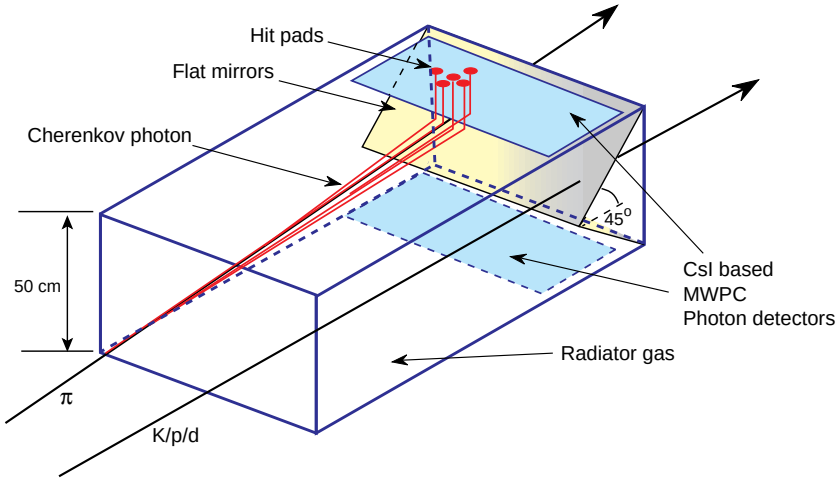

Figure 4: Schematic layout of a TIC detector. Two particles are traversing the gas radiator, one of them emits Cherenkov photons since it is above the Cherenkov threshold.

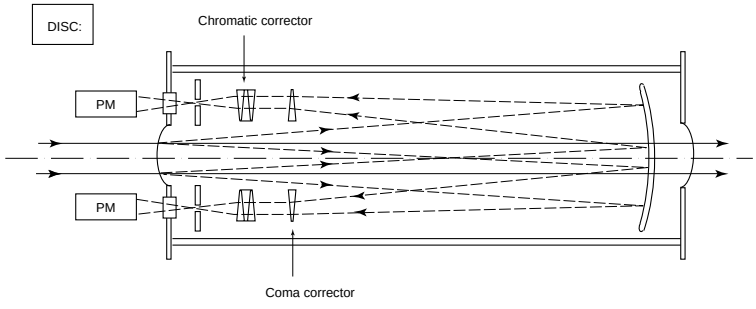

Figure 5: Schematic layout of a DISC counter. The spherical mirror shown on the right hand side focuses Cherenkov light onto a phototube matrix through a correcting optics and a ring diaphragm.

compensating the chromatic dispersion of the radiating medium (Fig. 5). PID is achieved by requiring the coincidence of several photomultipliers, therefore the efficiency ϵ_k for a k-fold coincidence is

$$\epsilon_k = (1 - e^{-n_{p.e.}/k})^k, \tag{11}$$

where $n_{p.e.}$ is the number of detected photoelectrons.
Consequently, the overall efficiency rapidly decreases by requiring more photomultipliers in coincidence, it never reaches 90% even in the case of a large number of detected photoelectrons, although the detector capability of rejecting unwanted particles is always very high as mentioned before. As for drawbacks, DISCs are quite complicated devices and are utilized only to tag the particles belonging to primary beams; therefore, although they have the best performance of all Cherenkov detectors, the limited phase-space acceptance makes them of no practical use for identifying secondary particles.

4.3 RICH detectors

The small angular coverage of DISCs was overcome by the RICH counters which allow simultaneous measurement of the values of β for several particles of different known momentum by determining the position of a certain number of Cherenkov photons. In a RICH detector, Cherenkov radiation, emitted from several particles in the same event, is transmitted through an optics, that could be either focusing with a spherical (or parabolic) mirror or not focusing (proximity-focusing), onto a photodetector that converts photons into photoelectrons with high spatial and time resolutions. Cherenkov footprints are visualized onto the plane of detection thus allowing the determination of the emission angle θ_c for each detected photon. The mass m of the particle of known momentum p is eventually given by

$$m = p\sqrt{n^2 \cos^2 \theta_c - 1}\ . \tag{12}$$

5 Design criteria of RICH detectors

The great challenge of the RICH technique is the detection of signals of single electrons, i.e. analogous to the detector "noise". Therefore, a careful design is mandatory for achieving the best detector performance.

As previously mentioned, a RICH detector consists of two basic elements arranged in a focusing or in a proximity-focusing geometry: a transparent dielectric medium, called the radiator, whose refractive index is appropriate for the range of particle momentum being specifically studied (Eq. 2) and a photon detector. The latter provides information on the position of the photoelectron initiated by the conversion of the Cherenkov photons in a suitable photosensitive volume, or a conversion layer. The focusing arrangement (Fig. 6) is more suited for low refractive index radiators (mainly gas) due to the long length needed to provide a satisfactory number of detected photoelectrons per ring, whilst in the 'proximity-focusing' geometry (Fig. 7), a thin slab of radiator emits Cherenkov photons along a conical wavefront that enlarges in an inert gas volume between radiator and photodetector. The resolution of the Cherenkov rings is determined by the ratio of radiator thickness and photodetector distance. Quite compact designs are possible. In this configuration, the resolving power is worse than that for gaseous radiators, but it enables good PID in a momentum range where gaseous radiators are insensitive.

The design of a Cherenkov detector relies on Eq.(1), (3) and (7) and on the knowledge of the optical properties of the medium. Moreover, since Cherenkov radiation

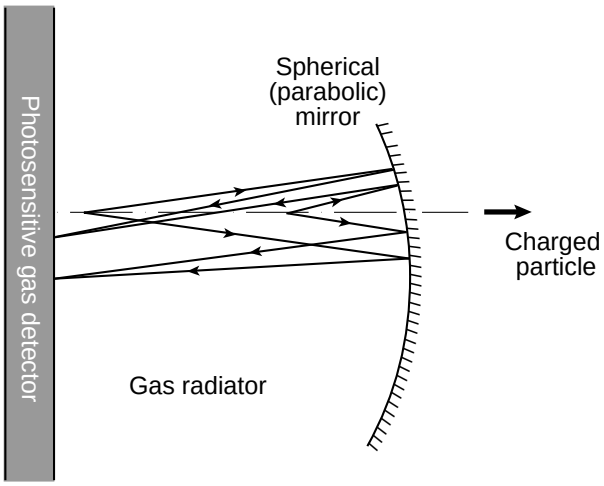

Figure 6: Focusing scheme: Cherenkov photons, collected by a mirror of focal length f, are focused onto the photon detector placed at the focal plane of the mirror. The resulting pattern is a circle of radius $r = ftan\theta_c$ regardless of the photon emission point along the particle track.

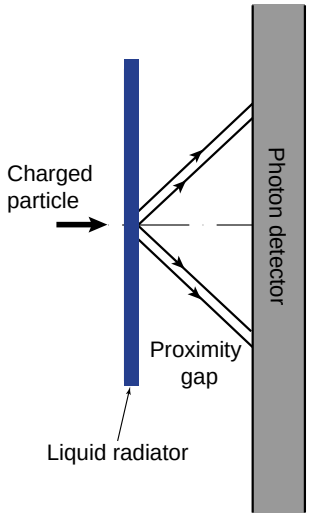

Figure 7: Proximity-focusing scheme: The detector volume, placed between the radiator and the photodetector, is known as the 'proximity gap' and is necessary to enlarge the Cherenkov cone to a more convenient size for the imaging.

is linearly polarized with its electric vector lying in the plane defined by the particle direction and the photon direction, special care must be taken in evaluating the reflection losses at the medium interfaces and in choosing materials fully isotropic to polarized light.

In any practical case, the medium transparency and photon detector inefficiencies allow only a few Cherenkov photons to be detected. Indeed, for a photon detector with quantum efficiency Q, single-electron detection efficiency ϵ, a transmission of radiator and windows T, and a mirror reflectivity (if present) R, the proportionality factor N_0, called the *figure of merit*, is defined as

$$N_0 = \frac{\alpha}{\hbar c} \int \epsilon Q\, T R\, dE\ . \tag{13}$$

The energy limits in the integral are defined on the bottom edge by the photoionization threshold and on the top edge by the medium transparency. The larger the N_0, the better the detector.
If a detector is designed to detect photons in a spectral region far from where the radiating medium has absorption bands, n can be taken to be independent of frequency, and the traditional equation used to describe Cherenkov counters results:

$$N = N_0 L \sin^2\theta. \tag{14}$$

The quantity given by Eq.(14) is the mean or expected value of a Poisson distribution. For $\beta \to 1$ the Cherenkov angle tends to the asymptotic value $\theta_{\max}$ related to threshold $\gamma_{\rm t}$ (Eq. 2) as

$$\sin^2\theta_{\max} = \frac{1}{\gamma_{\rm t}^2} \tag{15}$$

with a maximum expected number of detected Cherenkov photons

$$N_{\max} = \frac{N_0 L}{\gamma_{\rm t}^2}. \tag{16}$$

The fraction of Cherenkov photons at a given angle over the maximum yield is therefore expressed by

$$\frac{N}{N_{\max}} = \frac{\sin^2\theta}{\sin^2\theta_{\max}}. \tag{17}$$

For gas radiators, the following approximate expression is valid:

$$\frac{\sin^2\theta}{\sin^2\theta_{\max}} \simeq \frac{\theta}{\theta_{\max}} \simeq 1 - \frac{p_{\rm th}^2}{p^2} \tag{18}$$

implying that the Cherenkov angle and the number of detected photons depend in a universal way on the quantity $p/p_{\rm th}$. In Fig. 8 both the number of photons normalized to the asymptotic value $N_{\max}$ and the relative deviation of the Cherenkov angle from the asymptotic value are plotted against this scaling variable. The upper limit in the momentum range for particle discrimination is determined by the several sources of errors which limit the accuracy of the Cherenkov angle measurement. A complete discussion on this issue can be found in Ref.[2].

From Eq.(1), it derives:

$$\left(\frac{\sigma_\beta}{\beta}\right)^2 = (tan\theta\sigma_\theta)^2 + \left(\frac{\Delta n}{n}\right)^2. \tag{19}$$

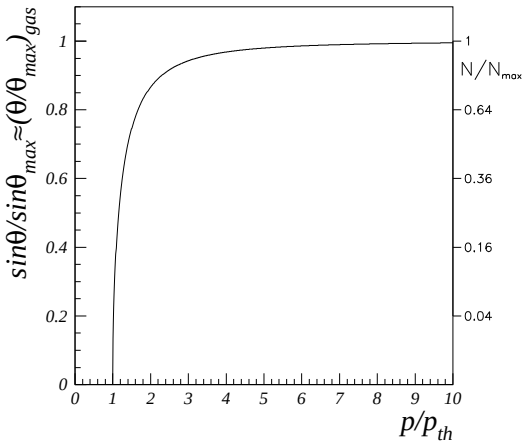

Figure 8: Variation of the Cherenkov angle sine and the number of photons normalized to their respective maximum values as a function of the scaling variable $p/p_{\rm th}$. In the case of a gas radiator the normalized ratio of the Cherenkov angle sines corresponds to the ratio between the Cherenkov angle and its maximum value. It is important to note that the maximum angle is reached much faster than the maximum number of photons as the particle momentum increases.

The spread in particle direction due to the multiple scattering in the radiator, the finite spatial resolution of the photon detector and the aberration of the optics used allow a spread of angles $\Delta\theta_i$ to be detected. The chromatic aberration of the radiating medium, $\Delta n/n$, is usually the dominant contribution to the detector precision σ_β/β, especially if the RICH detector is designed to be operated in the ultraviolet region. As an example, a gas radiator has a chromatic dispersion in the UV band almost twice that in the visible region. These contributions are independent and add in quadrature: ${\sigma_\theta}^2 = \Sigma_i {\Delta\theta_i}^2$. Since each detected photoelectron gives a separate measurement, for N photoelectrons, the Cherenkov angle resolution is improved:

$$\sigma_{\theta_{\rm c}} = \frac{\sigma_\theta}{\sqrt{N}}. \tag{20}$$

A RICH detector with a figure of merit N_0 and a radiator characterized by the refractive index n and total length L measures the Cherenkov angles θ_1 and θ_2 of two particles of momentum p and masses m_1 and m_2 respectively, with an accuracy described by the number of standard deviations n_σ such that $\theta_2 - \theta_1 = n_\sigma \sigma_{\theta_c}$. From Eq.(9) it follows that the upper momentum limit p_{m_1,m_2} for n_σ standard deviation separation is

$$p_{m_1,m_2} = \left(\frac{\Delta m^2 (N_0 L)^{\frac{1}{2}}}{2 n_\sigma \, \beta \, n \, \sigma_\theta} \right)^{\frac{1}{2}} = \left(\frac{\Delta m^2}{2 n_\sigma \, \beta \, n \, \sigma_{\theta_c} sin\theta} \right)^{\frac{1}{2}} = \left(\frac{\Delta m^2 \sqrt{N}}{2 n_\sigma \, \sigma_\theta tan\theta} \right)^{\frac{1}{2}}. \tag{21}$$

In Fig. 9, the upper momentum limit is plotted as a function of Cherenkov angle resolution for three different values of n_σ in the case of a proximity-focusing detector employing a 1 cm thick layer of low-chromaticity C_6F_{14} liquid as radiator (with $n = 1.28$ at $\lambda = 175$nm). The lower momentum limit is due to the decreasing number of detected photons towards

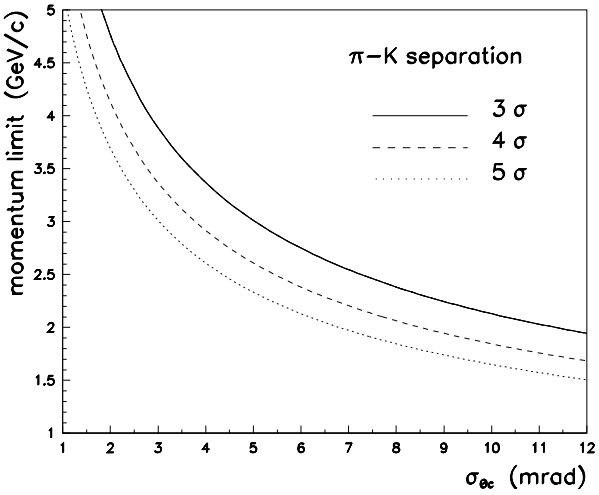

Figure 9: Estimated maximum momentum limit for a given Cherenkov angle resolution. A proximity-focusing RICH with $L = 1$ cm liquid perfluorohexane ($n = 1.28$ at $\lambda = 175$ nm) has been considered.

threshold (Eq. 17) since it has immediate consequences on the pattern recognition.

A good RICH design allows the value of p_{m_1,m_2} to be extended as far as possible once n_σ has been fixed by physics requirements on the desired PID efficiency and the allowed contamination. By assuming that a Gaussian distribution is applicable to the measured Cherenkov angles, a particle contamination smaller than 1% requires a separation power larger than $n_\sigma = 4$, and of course if the ratio between the two particle populations is 1 to 10 then the actual contamination of the largest populated sample of particles in the other species is ten times larger, i.e. 10% for $n_\sigma = 4.2$.

Equation (21) entails that the largest momentum limit is achievable by increasing N_0 and decreasing σ_θ. These two parameters are correlated with each other. Indeed the new direction in the technique of Cherenkov light imaging is focused on achieving main advantages on both operational aspects and performance by designing RICH detectors that operate in the visible light region [16]. In fact, at longer wavelengths the detector figure of merit is larger due to the enlarged bandwidth for the relevant photoelectron yield (higher material transparency) and the angular accuracy for the single photon is smaller due to the reduced chromatic aberrations of materials in the visible region. In the following the detector components are analysed in the light of the most recent technological advances.

6 Detector components

6.1 Photon detector

The basic task of the photon detector is to convert Cherenkov photons into a detectable electrical signal by means of a material with a high single-photon sensitivity defined by the quantum efficiency QE.

The low energy of the Cherenkov quanta implies that among the three interaction mechanisms of photons with matter, photoelectric absorption, Compton scattering and pair production, only the first one can be efficaciously exploited for practical purposes. Moreover it also implies that the photon detector must be able to detect with high ef-

ficiency the single electrons (photoelectrons) kicked off the atoms of the implemented photosensitive material that could be either a vapour (in this case the photoelectron production mechanism is called photoionization) or a thin solid layer (where more properly one refers to photoelectric production).

Besides the above-mentioned characteristics, the photon detector employed in a RICH device must also have:
- high localization accuracy able to match the errors in the Cherenkov angle;
- fast response;
- low noise;
- long-term stability;
- low cost in order to cover large surfaces.

Photon detectors can be divided into two classes: gaseous and vacuum-based detectors.

6.1.1 Gaseous photon detector

This class gathers together multiwire proportional chambers (MWPC), multistep avalanche chambers (MSAC) and drift chambers with two-dimensional properties.

The pioneering work of T. Ypsilantis and J. Seguinot has shown that building such detectors is completely realistic by using vapours with a high QE in the UV region [17]. The produced photoelectrons are detected by accelerating them in a uniform electric field towards a wire a few tens of μm thick at high voltage. Close to the wire the electric field is very high and gives the drifting electrons enough energy to create an avalanche by knocking secondary electrons out of the gas atoms. The resulting ionization is large enough to be detected by a cathode electrode subdivided into pads and instrumented with sensitive electronics. Pad address gives an ambiguity-free two-dimensional image, allowing the reconstruction of overlapping rings from a multiparticle event.

At moderate amplification gain ($1-5\cdot10^5$), single-electron pulse-height distribution has an exponential shape. In fact in the case of low electric field, the electron ionization is built up with several independent collisions with the gas atoms and therefore the probability $P(q)$ that an avalanche has a charge q is obtained by the Furry distribution:

$$P(q) = \frac{e^{-q/\overline{q}}}{\overline{q}} \ , \tag{22}$$

where $\overline{q}$ is the mean charge of the avalanche.
The single-electron detection efficiency is therefore given by:

$$\epsilon = \int_{q_{th}}^{\infty} P(q)dq = e^{-q_{th}/\overline{q}}, \tag{23}$$

where q_{th} is the threshold charge needed to remove the detector noise. The exponential form of ϵ is an unfavourable feature of gas detectors operated at low gains. In fact, a small decrease in the gas amplification implies a strong loss of efficiency. A more favourable pulse-height distribution (called the Polya distribution) occurs for higher gain values [18]:

$$P(q) = \left(\frac{q(1+\theta)}{\overline{q}}\right)^{\theta} exp\left(\frac{-q(1+\theta)}{\overline{q}}\right), \tag{24}$$

where the empirical parameter θ is related to the gas amplification mechanism. The Polya distribution takes the simple exponential form of the Furry distribution for $\theta = 0$ (Fig. 10),

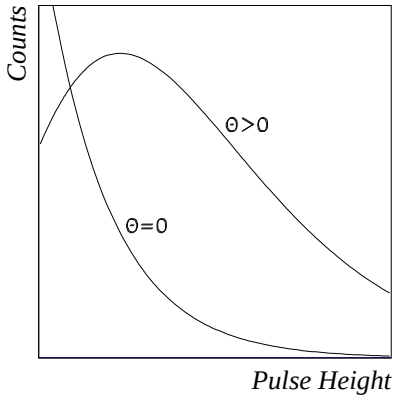

Figure 10: Qualitative behaviour of the single photoelectron pulse-height distribution for high ($\theta > 0$) and low ($\theta = 0$) gas amplification gains.

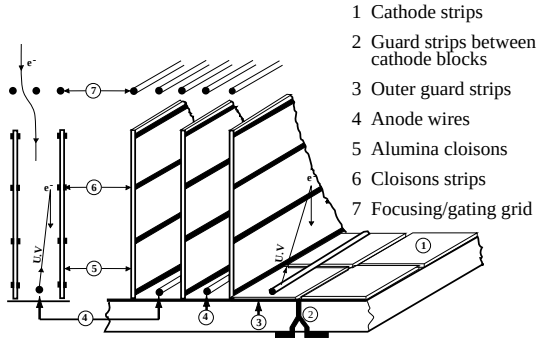

Figure 11: Schematic diagram of the blinds between anode wires used in the DELPHI RICH photon detector to control the photon feedback phenomenon.

condition reached by decreasing the electric field. The peaked pulse-height distribution allows a more stable setting of the electronic threshold, but at higher gains the gas photon detectors experience a positive photon feedback caused by photons emitted by the de-excitation of gas molecules after the avalanche mechanism has occurred. Secondary photons initiate new avalanches after being converted by the photosensitive agent in the chamber. Blind electrodes are then implemented in order to shield the sensitive volume from the main avalanches (Fig. 11). Photon feedback is a clear limitation to the chamber gas gain. In fact, the light output from the avalanches grows exponentially as the chamber gain is increased beyond plateau.

Although benzene was used as a photosensor in the early prototypes, it was immediately replaced by photosensitive vapours with a lower photoionization threshold such as triethylamine (TEA) or tetrakis(dimethylamine)ethylene (TMAE) added to a regular gas mixture and flushed through the detector volume. As shown in Fig. 12, TMAE has a higher QE than TEA due to the strong electron donor properties of the attached dialkylamino groups (Fig. 13). The higher photoionization threshold of TEA (7.2 eV) severely

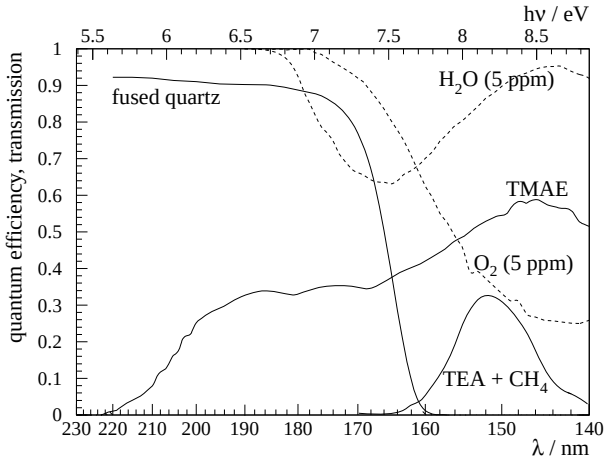

Figure 12: TEA and TMAE quantum efficiency as a function of the photon wavelength. Also shown are the transmission plot of a fused silica and the limit of transparency when 5 ppm of water and O_2 impurities are present in the gas volumes.

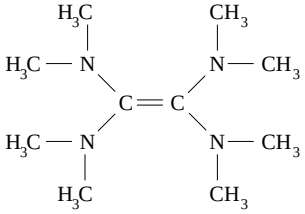

Figure 13: TMAE chemical structure.

restricts the choice of materials that can be used as UV windows, therefore fused silica that has transparency characteristics valid for TMAE must be replaced by more expensive CaF_2 windows. Moreover, extraordinary care must be taken to keep the contamination level of water and oxygen, which absorb strongly in the UV, below 1 ppm in the gas volumes (radiator and drift gas), in order to avoid a reduction of detected photons (Fig. 12). In contrast to TEA, whose vapour pressure is 52 Torr at room temperature with an absorption length of 0.61 mm, TMAE vapour pressure of 0.30 Torr at room temperature is a disadvantage because it results in a long photon absorption length (3 cm) and therefore a large parallax error. Although the chemical reaction products of TMAE are highly electronegative and therefore absorb photoelectrons, the careful design of the detector and gas-handling system, and operation at higher temperatures adopted by the largest systems so far built (OMEGA [19], DELPHI [20] and SLD [21]) have enabled to reach large enough TMAE concentrations and stable operation.

An interesting feature of TMAE is its capability to emit light in the visible region as a result of the de-excitation of excited states formed by electron impact collisions with its molecules [22], during the avalanche amplification process in gaseous chambers. This excited state is caused by three basic mechanisms: photoabsorption, energy transfer from excited noble gas dimer and direct excitation by accelerated electrons [23]. The ratio of the amount of light produced to the amount of charge present is a function of the charge gain and light is more efficiently produced at low charge gain. The NA35 experiment exploited the light emission by TMAE in its optically read out RICH [24].

In recent years, a considerable effort has been made to prove that a thin film (100 nm $\div 1$ μm) of CsI deposited onto the cathode plane of a gaseous detector is a valid alternative to the use of TMAE in large-area RICH detectors.
A specific R&D programme for the development of large-area CsI photocathodes was approved in 1992 by the DRDC at CERN under the name RD26 [25].
RD26 achieved a breakthrough in CsI deposition techniques by developing a successful standardized technology of evaporating photocathodes, as large as 50×50 cm^2, without the expensive and time-consuming implementation of masking techniques [26].

At CERN, the photocathodes are prepared in a large evaporation stand equipped with four DC heated tungsten crucibles operated simultaneously to achieve a uniform CsI layer. The best CsI quantum efficiency (Fig. 14) is obtained by depositing at least 250 nm of CsI onto a printed circuit board with a copper layer, accurately prepolished by mechanical and chemical treatments, and subsequentely covered with a thick (7 μm) chemically-deposited nickel layer, followed by a thinner (0.5 μm) layer of gold [29]. During the deposition, the pad substrate is held at 50°C. A 12-hour post-deposition heat treatment at 60°C, under vacuum, is necessary in order to achieve the final CsI QE [30] (Fig. 15).
In the near future, three experiments will implement a CsI RICH detector in their layout. Two of them (HADES [31] and COMPASS [32]) are building a system with a focusing scheme, whilst the third one (ALICE [33]), is envisaging a proximity focusing geometry.

The main advantages of a CsI RICH detector are an improved Cherenkov angle resolution since photoconversion is achieved in a single layer without parallax error, and a simplified structure owing to the suppression of the photon detector window employed in the case of a TMAE RICH. This results in considerable cost-saving and a reduced total radiation length.
The possibility of using a thin anode-cathode gap (4 mm) (Fig. 16) simplifies the cumbersome Cherenkov pattern recognition in a high multiplicity environment because the

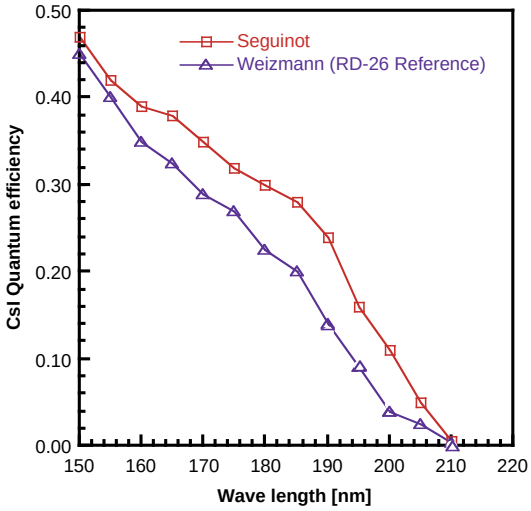

Figure 14: Measurements of CsI quantum efficiency in vacuum as a function of the photon wavelength performed by Seguinot et al [27] and A. Breskin et al. [28].

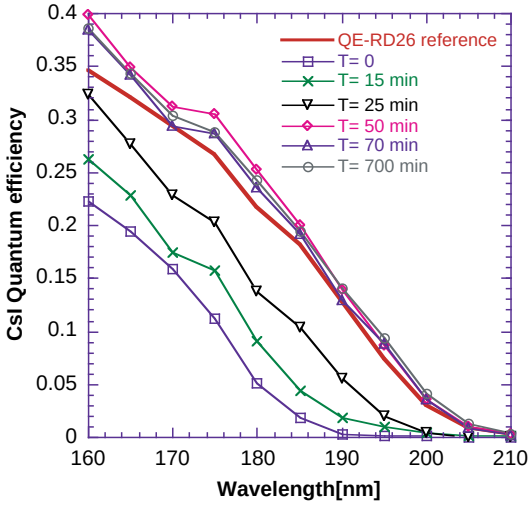

Figure 15: Heat treatment effect on QE of a CsI sample after evaporation at 60°C kept under vacuum.

chamber geometry approaches the ideal 2-D geometry and, furthermore, it reduces the background since ionizing particles traverse a small sensitive volume. These features are particularly mandatory in the case of ALICE RICH since an average multiplicity per event larger than 50 primary particles/m^2 is anticipated for LHC $Pb-Pb$ central collisions. A relevant feature of the photon detector shared by all the three CsI RICH designs

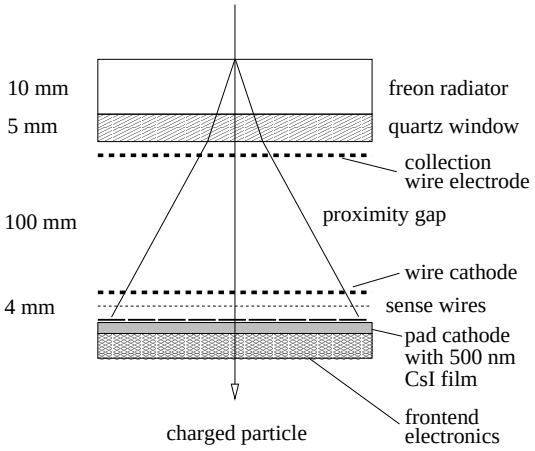

Figure 16: Schematic layout of the fast ALICE CsI RICH. The photodetector is a multiwire proportional chamber (MWPC), with anode wires of 20 μm diameter, 4 mm pitch and 2 mm anode-cathode gap. The MWPC is filled with pure methane at ambient temperature and pressure. Electrons released by ionizing particles in the proximity gap are prevented to enter the MWPC volume by a positive polarization of the electrode close to the radiator. A low noise and highly multiplexed VLSI analog electronics is fully integrated on the rear of the cathode plane, enabling the determination of the hit coordinates by centroid measurements.

is the "open geometry" i.e. the suppression of blinds that in TMAE photodetectors are specifically implemented to prevent spurious avalanches from feedback photons. In fact, the expected negligible background level from the CsI layer does not require any complex electrode structure [33].

6.1.2 Vacuum-based photon detectors

Already in the past, RICH systems were succesfully designed and built to operate in the visible light region [34, 35]. More recently, advances in technologies associated with the detection of visible light with devices of high granularity have stimulated fruitful new ideas [16]. With respect to the detector operational aspects, the main benefits are as follows:
- no special handling for nasty photosensitive vapours such as TMAE;
- modest service and maintenance needs;
- savings in operating costs since gas circulation systems and expensive UV windows are no longer necessary;
- high segmentation flexibility and compactness.
The detector performance improves as follows:
- high rate capability and availability of the detector for triggering;
- a larger choice of materials as radiator, in particular the possibility of using aerogel (Section 6.2);

- removal of background caused by incoming neutrons (neutrons create spurious hits in the hydrogenous gas mixtures used in RICH photon detectors as a consequence of proton recoils).

In 1991, T. Sugitate et al. [34] reported results from successful detection tests of Cherenkov rings focused onto an image intensifier coupled to a CCD camera. Although this technique seems very promising, CCDs are small and quite slow devices. This last constraint is severe, and in fact the acquisition rate of RICH detectors, barely relevant a few years ago, has now become a crucial issue.
The phototube (PMT) has the merits of robustness, low noise, high gain, and high rate capabilities, but it is sensitive to magnetic fields. "Quantacon-like" PMTs have a high single-photoelectron efficiency but a high cost per channel. A powerful application is represented by the experiment SELEX at Fermilab where almost 3000 PMTs have been employed to detect the Cherenkov light from a gaseous RICH device [35, 36]. The experiments PHENIX [37] and BABAR [38] also detect the Cherenkov light with an array of PMTs.

In large-area applications, the multianode PMT (MaPMT) is more suitable since it offers the advantage of many channels with a single common power supply and a compact readout. MaPMTs, first used by S. Endo et al. [39], are now the baseline photodetectors for the Hera-B RICH [40]. The commercial tubes have a crosstalk of much less than 1% and a pad-to-pad variation in gain of less than 30% [41]. Use in a magnetic field of over 1.5 T is possible using fine mesh tubes, although at a high cost and with lower single-photon sensitivity.

Recently, hybrid photodevices have made considerable progress since their 'rediscovery' to the stage where they are now being proposed in the LHCb experiment at LHC [42], as an alternative to the MaPMT and in the long baseline neutrino experiment AQUARICH [43]. They consist of an array of silicon pin diodes placed in a vacuum tube with a standard transmission photocathode kept at a negative voltage of several KV with respect to the silicon. Photoelectrons are accelerated by the electric field and penetrate

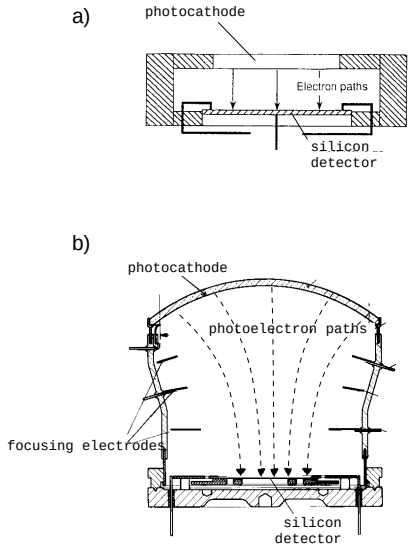

Figure 17: Different geometries of HPD detectors: a) proximity focusing, b) electrostatic focusing.

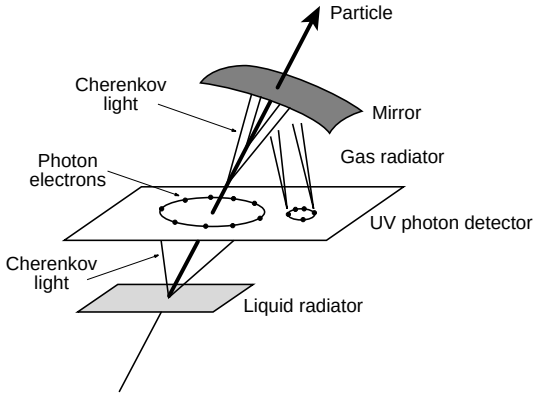

Figure 18: A schematic of a dual radiator RICH: the UV photon detector visualizes rings from both the liquid radiator and the gas radiator.

the solid state diodes where thousands of electron-hole pairs are developed. Two electric field configurations are possible: proximity focusing and electrostatic focusing (Fig. 17). The latter has a small detector dead area but is very sensitive to magnetic fields. HPDs potentially offer outstanding features like high spatial resolution, stable gain, a wide dynamic range and an excellent single photoelectron response [44]. Nevertheless, for large area RICH device applications more R&D for implementing the FE electronics in vacuum is needed in order to avoid the large number of feedthrough lines. In addition, the commercially-available devices, in spite suitable performances, suffer from a large inactive area and high cost. The development of cheap hybrid devices with a large active area is presently underway at CERN [45].

Finally, it is worthwhile mentioning the Visible Light Photon Counters (VLPCs) because of their very high QE (85% for green light). VLPCs are based on doped SiAs crystals cooled at 7 K, biased at low voltage. Visible photons are guided through glass fibres into the intrinsic region of the detector where they create electron-hole pairs [46]. The resulting impact of one electron on a neutral crystal impurity starts an electron avalanche. Although they run with a speed of up to 30 MHz, the need of a cryogenic system and high costs have prevented them from being implemented in actual experiments so far.

6.2 Radiator

The particle identification momentum range determines the choice of the radiator medium and a dual radiator geometry, i.e. a detector with both focusing and proximity focusing geometries, is in many cases mandatory to cover an extended momentum range for particle identification (Fig. 18). The choice of materials available able to feature as a Cherenkov radiator is quite limited. Since the intensity of the Cherenkov light emitted is much smaller than that given off in the scintillation process, an important requirement placed upon a radiator material is that it should not scintillate appreciably. Moreover, it must not have absorption bands in the wavelength range to be used.

The radiator volumes must be isolated from the photon detector, and at the same time, photons must be able to travel across the boundary with little loss. Since most of the Cherenkov light is emitted in the far ultraviolet region, (Eq.(6), where the λ^{-2} dependence is explicitly given), only a few substances are sufficiently transparent to permit good Cherenkov light transmission. Therefore, the choice of radiator is limited even further,

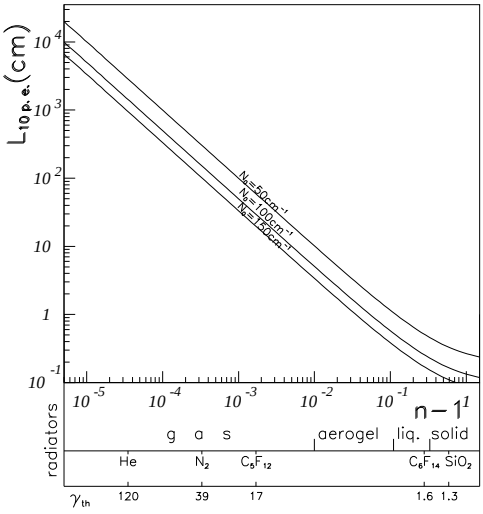

Figure 19: Radiator length corresponding to a yield of 10 photoelectrons as a function of the index of refraction of the medium for different RICH figures of merit.

particularly for liquid radiators.
UV transparency reduces the choice of window materials to: lithium fluoride, magnesium fluoride, calcium fluoride, natural quartz and fused silica. The latter is the only feasible choice in large RICH detectors, because it can be fashioned into large flat sheets, it has a high resistance to radiation and very good transparency, up to wavelengths of 160 nm (i.e. energy below 7.5 eV).

The radiator length required to produce at least 10 photoelectrons in a RICH detector with a given figure of merit is plotted in Fig. 19 as a function of the refractive index of the chosen medium.

Silica aerogel is the only existing material with optical properties suitable for filling the gap in the refractive index between liquids and heavy gases.
Aerogel is a manmade material that can have a density as low as three times that of air. It essentially consists of grains of amorphous SiO_2 with sizes ranging from 1 to 10 nm, linked together in a three-dimensional structure filled by trapped air. The huge number of such tiny primary particles determines an internal surface close to 1000 m^2/g which plays a fundamental role in the aerogel chemical and physical behaviour. There exists a simple relationship between the resultant index of refraction and the aerogel density ρ in g/cm^3[47]:

$$n = 1 + 0.21\rho \ . \tag{25}$$

Density values lying between 0.003 g/cm^3 and 0.55 g/cm^3 are in principle available, corresponding to the refractive indices of n=1.0006 ($\gamma_t = 29$) and n=1.11 ($\gamma_t = 2.3$), respectively.

The granular structure of aerogel with a typical length scale of a few nm determines its optical properties. The behaviour of visible light in aerogel is dominated by Rayleigh scattering which increases as the fourth power of the frequency. When Rayleigh scattering occurs, the directionality of the Cherenkov radiation is completely lost. Therefore, the major concern associated with the design and construction of a RICH detector with an

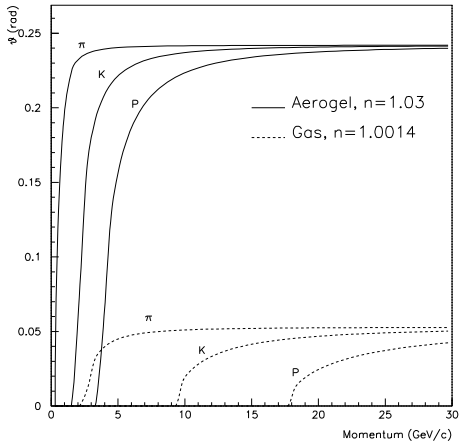

Figure 20: Momentum range covered by a RICH device with two radiators: gas C_4F_{10} and aerogel with n=1.01

aerogel radiator is whether the Cherenkov photons that traverse the aerogel without any scattering are sufficient in number to allow the measurement of their emission angle with the expected accuracy.
Simple calculations show that the useful production of Cherenkov light is limited to the visible region.
Recently, hydrophobic, crack-free, very transparent aerogel samples became routinely available [48]. Loss of photons due to absorption and scattering processes in the bulk material has been minimized, as observed in test beam studies [49].
The "breakthrough" in the fabrication of aerogel has promoted more advances in the use of this material in Cherenkov detectors, as V.I. Vorobiov [50] and H. v. Hecke [51] pointed out in 1991 and 1993, respectively. Nonetheless, the major merit of the rapid progress of aerogel in real RICH devices must be ascribed to J. Seguinot and T. Ypsilantis who revised the van Hecke proposal in the light of currently available photodetector technology and envisaged an appealing application in the LHCb experiment [52]. Their design also inspired the upgrading of HERMES at DESY [53].
Both experiments use a dual radiator RICH with aerogel (n=1.03) and gas C_4F_{10} (Fig. 20).

7 Conclusions

A phenomenon discovered by the Russian scientist Cherenkov in 1934 has become in recent years the basic ingredient of the RICH devices able to identify particles in the vast momentum range $1 - 800$ GeV/c. To be successfully exploited the Cherenkov radiation imaging technique requires a skilful team of physicists and engineers since many parameters must be controlled and mantained during the operation of the detector. Despite their complexity and high manpower costs, the outstanding physics results that have been achieved from the first generation of large RICH devices largely compensate the efforts made and justify the construction of new devices for future experiments.

8 Acknowledgements

I wish to thank S. Majewsky, T. Ekelof and the Director of the VIII ICFA School on Instrumentation, Prof. M. Nizamettin Erduran, for having invited me to such an enjoyable and stimulating school.

References

[1] A. Roberts, Nucl. Instr. and Meth. 9 (1960) 55;
S.K. Poultney et al., Rev. Sci. Instr. 33 (1962) 574.

[2] J. Seguinot, CERN-EP/89-92;
T. Ypsilantis and J. Seguinot, Nucl. Instr. and Meth. A 343 (1994) 1-29 and 30-51.

[3] The Proceedings of the 1st, 2nd and 3rd RICH Workshops have been published in Nucl. Instr. and Meth. A 343 (1994), A 371 (1996) and A 433 (1999), respectively.

[4] O. Heaviside, Electrical Papers, II, 494 (Macmillan, London, 1892).

[5] P.A. Cherenkov, Acad. Sci. URSS, 2, 451 (1934); see also Phys. Rev. 52 (1937) 378 for English language publication of Cherenkov early work.

[6] I.M. Frank and I.J. Tamm, Dokl. Academie des Sciences de l'URSS, 14 (1937) 107.

[7] V.L. Ginzburg, Zh. Eksp. Teor. Fiz. SSSR, 10 (1940) 589.

[8] P.A. Cherenkov, Izv. Akad. Nauk. SSSR, Ser. Fiz. OMEN, 1 (1937) 455.

[9] J.V. Jelley, Progress in Nuclear physics, 3 (1953) 131.

[10] O. Chamberlain et al., Phys. Rev. 100 (1955) 947.

[11] J. Seguinot and T. Ypsilantis, Nucl. Instr. and Meth. 142 (1977) 377.

[12] J. Seguinot and T. Ypsilantis, Nucl. Instr. and Meth. A 343 (1994) 1.

[13] M. Adams et al., Nucl. Instr. and Meth. 217 (1983) 237.

[14] C. W. Fabjan et al., Nucl. Instr. and Meth. A 367 (1995) 240.

[15] J. Litt and R. Meunier, Ann. Rev. Nucl. Sci. 23 (1973).

[16] E. Nappi, Nucl. Instr. and Meth. A 409 (1998) 417;
J. Seguinot and T. Ypsilantis, Nucl. Instr. and Meth. A 433 (1999) 1.

[17] J. Seguinot et al., Nucl. Instr. and Meth. 173 (1980) 283;
T. Ekelof et al., Phys. Scripta 23 (1981) 718.

[18] J. Byrne, Proc. R. Soc. Edinburgh 66A (1962) 33.

[19] U. Muller et al., Nucl. Instr. and Meth. A 371 (1996) 27.

[20] W. Adam et al., Nucl. Instr. and Meth. A 371 (1996) 12.

[21] K. Abe et al., Nucl. Instr. and Meth. A 371 (1996) 8.

[22] G. Charpack et al.,Nucl. Instr. and Meth. A 258 (1987) 177.

[23] M. Suzuki et al., Nucl. Instr. and Meth. A 254 (1987) 556.

[24] J. Baechler et al., Nucl. Instr. and Meth. A 343 (1994) 213.

[25] E. Nappi et al., RD26 proposal to DRDC, CERN/DRDC 92-3 and ADDENDUM to the DRDC PROPOSAL P35, CERN/DRDC/92-16.

[26] E. Nappi et al., Status report of the CsI-RICH Collaboration, CERN/LHCC 96-20;
F. Piuz, Nucl. Instr. and Meth. A 371 (1996) 96.

[27] J. Seguinot et al., Nucl. Instr. and Meth. A 297 (1990) 133.

[28] G. Malamud et al., Nucl. Instr. and Meth. A 343 (1994) 121.

[29] F. Piuz, Nucl. Instr. and Meth. A 433 (1999) 178.

[30] A. Buzulutskov at al., Nucl. Instr. and Meth. A 366 (1995) 410.

[31] HADES, Proposal for a High Acceptance Di-Electrons Spectrometer, GSI, Darmstadt, 1993.

[32] COMPASS proposal, CERN/SPSCL/96-14.

[33] ALICE TDR 1, CERN/LHCC 98-19.

[34] T. Sugitate et al., Nucl. Instr. and Meth. A 307 (1991) 265.

[35] M. Maia et al., Nucl. Instr. and Meth. A 326 (1993).

[36] J. Engelfried et al.,The SELEX Phototube RICH detector, Fermilab-Pub-98/299-E, hep-ex/9811001.

[37] PHENIX Conceptual Design Report, January 1993.
[38] B.N. Ratcliff, Nucl. Instr. and Meth. A 371 (1996) 309.
[39] S. Endo et al., A test of an improved RICH prototype, Institute for Nuclear Study (Tokyo) Annual Report, 1990.
[40] P. Krizan et al., Nucl. Instr. and Meth. A 387 (1997) 146.
[41] Y. Yoshizawa and J. Takenchi, Nucl. Instr. and Meth. A 387 (1997) 33.
[42] LHCb Technical proposal, CERN/LHCC 98-4, LHCC/P4.
[43] Letter of Intent for Long Baseline RICH, CERN-LAA 96-01, T. Ypsilantis et al., Nucl. Instr. and Meth. A 371 (1996) 330;
P. Antonioli et al., Proceedings of the 36th Workshop on the INFN Eloisatron Project, Erice, Italy, 1-7 Nov. 1997 (World Scientific 1977).
[44] R. DeSalvo, Nucl. Instr. and Meth. A 387 (1997) 92.
[45] A. Go et al., Nucl. Instr. and Meth. A 433 (1999) 153.
[46] M.D. Petroff and M. Atac, IEEE Trans. Nucl. Sci. NS-36 (1989) 163.
[47] G. Poelz and R. Reithmuller, Nucl. Instr. and Meth. 195 (1982) 491.
[48] I. Adachi et al., Nucl. Instr. and Meth. A 355 (1995) 390.
[49] R. De Leo et al., Nucl. Instr. and Meth. A 401 (1997) 187.
[50] V.I. Vorobiov et al., Proc. of the Workshop on physics and detectors for DAPHNE, report INFN-Frascati, 1991.
[51] H. van Hecke, Nucl. Instr. and Meth. A 343 (1994) 311.
[52] J. Seguinot and T. Ypsilantis, Nucl. Instr. and Meth. A 368 (1995) 229.
[53] R. De Leo et al., "Proposal to add a ring imaging Cherenkov detector to HERMES", INFN-ISS 96/9;
E. Cisbani et al., Progress report on the Feasibility studies of a RICH detector for HERMES, INFN-ISS 96.